Received: 22 July 2022 | Revised: 27 September 2022 | Accepted: 30 September 2022

DOI: 10.1111/mmi.14988

RESEARCH ARTICLE

WILEY

Enzyme 1 of the phosphoenolpyruvate:sugar phosphotransferase system is involved in resistance to MreB disruption in wild-type and Δ*envC* cells

Ryan Sloan | Jacob Surber | Emma J. Roy | Ethan Hartig | Randy M. Morgenstein

Department of Microbiology and Molecular Genetics, Oklahoma State University, Stillwater, Oklahoma, USA

Correspondence
Randy M. Morgenstein, Department of Microbiology and Molecular Genetics, Oklahoma State University, Stillwater, OK, USA.
Email: randy.morgenstein@okstate.edu

Funding information
National Institute of General Medical Sciences, Grant/Award Number: 1R15GM129636-01A1

Abstract

Cell wall synthesis in bacteria is determined by two protein complexes: the elongasome and divisome. The elongasome is coordinated by the actin homolog MreB while the divisome is organized by the tubulin homolog FtsZ. While these two systems must coordinate with each other to ensure that elongation and division are coregulated, this cross talk has been understudied. Using the MreB depolymerizing agent, A22, we found that multiple gene deletions result in cells exhibiting increased sensitivity to MreB depolymerization. One of those genes encodes for EnvC, a part of the divisome that is responsible for splitting daughter cells after the completion of cytokinesis through the activation of specific amidases. Here we show this increased sensitivity to A22 works through two known amidase targets of EnvC: AmiA and AmiB. In addition, suppressor analysis revealed that mutations in enzyme 1 of the phosphoenolpyruvate:sugar phosphotransferase system (PTS) can suppress the effects of A22 in both wild-type and *envC* deletion cells. Together this work helps to link elongation, division, and metabolism.

KEYWORDS
A22, cell shape, divisome, elongasome, MreB, phosphoenolpyruvate:sugar phosphotransferase system

1 | INTRODUCTION

Bacteria come in a variety of shapes and sizes that are determined by the peptidoglycan cell wall. One of the more common shapes is a bacillus, or rod shape. Rod shape is regulated by the actin homolog, MreB. In addition to MreB many proteins are needed to form and maintain a rod shape. Together these proteins are termed the elongasome and are made of penicillin binding proteins (PBP), SEDS proteins (shape, elongation, division, and sporulation) and different accessory factors, such as MreC, MreD, and RodZ (Alyahya et al., 2009; Bendezu et al., 2009; Cho et al., 2016; Kruse et al., 2005; Meeske et al., 2016; Morgenstein et al., 2015; Shi et al., 2018; Shiomi et al., 2008). MreB is thought to act as a scaffold to organize and direct the localization of the cell wall synthesis enzymes to maintain rod shape (Billings et al., 2014; Bratton et al., 2018; Lee et al., 2014; Ursell et al., 2014).

MreB is highly conserved among bacteria and can be found in both Gram-positive and Gram-negative species. MreB forms short polymers on the inner surface of the cytoplasmic membrane (Dempwolff et al., 2011; Kruse et al., 2005; Salje et al., 2011). Loss of *mreB* leads

Ryan Sloan and Jacob Surber contributed equally to this work.

to spherical cells that eventually lyse, unless grown very slowly (doubling times >100 minutes) or with suppressor mutations, such as the overexpression of the cell division genes, *ftsZAQ* (Bendezú & de Boer, 2008). To avoid accumulating suppressor mutations, the MreB depolymerizing agent A22 is often used to study the role of MreB in cell shape and physiology (Bean et al., 2009; Gitai et al., 2004).

We have previously explored conditions in which *Escherichia coli* cells are better able to withstand the loss of MreB function. Using A22 as a method for disrupting MreB we have shown that MreB and the elongasome in general are dispensable for growth but not cell shape once cells reach a threshold density (Grinnell et al., 2022). In addition, we have shown that mutations in metabolic genes that lead to an increase in cell wall precursors allow cells to better tolerate A22 treatment (Barton et al., 2021). To further understand the role of MreB in cell physiology we sought to find mutants that lead to an increase in sensitivity to A22 treatment.

Here, we used the Keio collection to find mutants that grow poorly in low levels of A22 and found that deletion of five genes result in reduced growth when MreB is disrupted (Baba et al., 2006). One of these genes, *envC*, is an activator of the cell wall amidases, AmiA and AmiB, which are needed for cell separation after division (Uehara et al., 2009, 2010). EnvC is part of the divisome, a separate cell wall synthesis complex used during cell division that is distinct from the MreB elongasome (Cho et al., 2014). We show that the increased A22 sensitivity is due to the lack of AmiA and AmiB activity and can be suppressed by mutations in *mreB* or deletion of enzyme 1 of the phosphoenolpyruvate:sugar phosphotransferase system (PTS). This work further connects central metabolism and cell size.

2 | RESULTS

2.1 | Deletions of diverse genes lead to A22 sensitivity

MreB is an essential protein for determining rod shape in many bacteria. It is conditionally essential for viability, as mutations that upregulate the cell division genes *ftsZAQ* or very slow growth can suppress the lethality of *mreB* deletions without restoring rod shape (Bendezú & de Boer, 2008). It is unknown if there are genetic conditions that make cells more susceptible to disruption of MreB. It is also unclear if MreB plays other roles in the cell, independent from regulating rod shape. We have previously reported that two gene deletions, *envC* and *tusE*, result in cells with increased sensitivity to A22, although the mechanism for this is unknown (Grinnell et al., 2022). Deletion of either of these genes leads to slower growth, a condition normally thought to promote growth without MreB (Figure S1) (Grinnell et al., 2022).

In order to determine if MreB has other cellular roles we performed a screen of the Keio collection, an ordered library of *E. coli* mutants, to find strains that are more sensitive to growth in low levels of A22, an MreB depolymerizing drug (Baba et al., 2006; Bean et al., 2009; Gitai et al., 2004). The Keio collection was grown in either LB medium or LB supplemented with a non-lethal amount of A22 (1 μg/ml). At this concentration of A22, wild-type (WT) cells grow close to the same rate as in LB alone (Figure S1); therefore, we looked for deletion strains that have reduced growth in A22 compared to LB alone to determine which, if any, gene deletions lead to increased sensitivity to MreB disruption. After three biological replicates, any deletion that had reduced growth in A22 compared to LB in more than one replicate was transduced from the Keio collection into MG1655, the WT *E. coli* strain used in our lab.

Five gene deletions were found to have an increased sensitivity to A22 (Table S1, Figure 1a). To further characterize this sensitivity, these strains were grown in low (1 μg/ml) or high (10 μg/ml) levels of A22 for 6 h. As the different mutant strains may have reduced growth rate in LB alone, the $O.D._{600}$ of cells grown in A22 was compared to growth in LB medium alone to produce a growth ratio. In this way we can measure the specific effect of A22 on growth for each strain. WT MG1655 cells grow to nearly the same density in 6 h in LB or low A22, producing a growth ratio ~0.9, but have about a 50% reduction in growth when grown in high levels of A22 (Figure 1a). All five strains from our screen display lower growth in high levels of A22

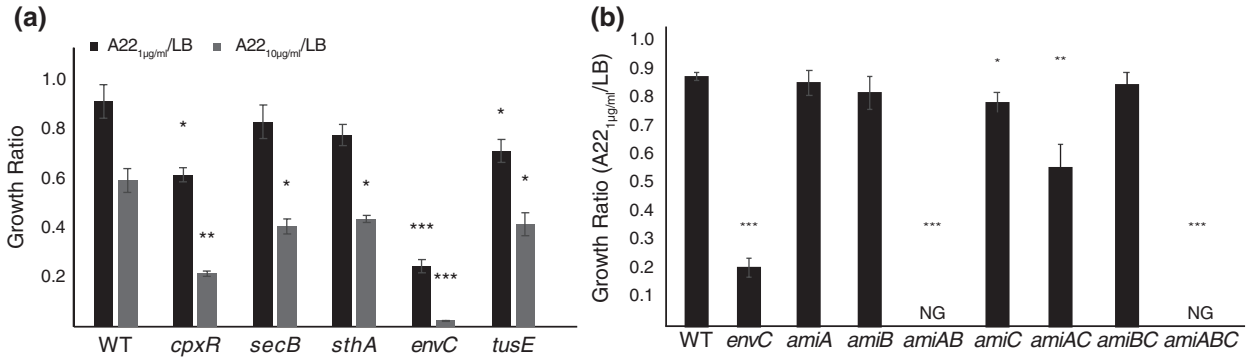

FIGURE 1 A22 sensitivity is increased in multiple gene deletions. Cells were grown for 6 h in LB or LB + A22. The ratio of $O.D._{600}$ between the two conditions was determined as a growth ratio. (a) The growth ratio was determined for WT (MG1655) and five gene deletions found through a screen of the Keio collection. Mutations were transduced into MG1655. (b) Growth ratios were determined for different strains related to cell separation after division. (a and b) Error bars are standard deviation from three independent biological replicates. $^{*}p < 0.05$, $^{**}p < 0.01$, $^{***}p < 0.001$.

with three stains also having reduced growth in low levels of A22. In support of our findings (*ΔsecB*), defects in the Sec system have been shown to cause increased sensitivity to A22 (Govindarajan & Amster-Choder, 2017). The *envC* mutant displays the most dramatic phenotype, with almost no growth in high levels of A22.

EnvC is an activator of cell wall hydrolases that are needed to separate daughter cells after division (Bernhardt & de Boer, 2004; Uehara et al., 2010). Due to the role of EnvC in cell division and therefore possible connection to MreB and the severe growth defect seen in both low and high levels of A22, we focused on determining why deletion of this gene leads to increased sensitivity to MreB disruption. To confirm that deletion of *envC* is responsible for the observed A22 sensitivity, we complemented *envC* on an arabinose inducible plasmid. Induction of plasmid-born *envC* fixes the growth defect in A22 (Figure S1).

2.2 | A22 sensitivity in the *envC* mutant is caused by the loss of AmiAB activity

EnvC works by activating two cell wall hydrolases, AmiA and AmiB (Uehara et al., 2010). To determine if the A22 sensitivity of the *envC* mutant is due to the lack of activation of AmiA and/or AmiB we made deletions of both genes individually and together. Deletion of either *amiA* or *amiB* alone has no effect on sensitivity to low levels of A22 (Figure 1b). However, the double deletion strain is even more sensitive to A22 than the *envC* deletion and did not grow at low levels of A22 (Figure 1b). This suggests that the sensitivity of the *envC* mutant to A22 is due to the lack of AmiAB activation and not a secondary role of EnvC.

AmiA and AmiB are not the only cell wall hydrolases in *E. coli* needed for cell separation after division. AmiC is a third hydrolase that is activated by the protein NlpD (Uehara et al., 2009, 2010). Because loss of *amiA* and *amiB* causes cells to become sensitive to A22, we tested whether loss of AmiC has any effect. Cells lacking AmiC show a mild increase in sensitivity to A22 (Figure 1b). We further analyzed double mutants of *amiAC* and *amiBC* as well as the triple *amiABC* mutant for A22 sensitivity. The *amiAC* mutant is even more sensitive than the *amiC* mutant alone, but not nearly as sensitive as either the *envC* deletion or *amiAB* mutant. As expected, the triple mutant shows an extreme sensitivity phenotype similar to the double *amiAB* mutant and did not grow in A22 (Figure 1b). These results suggest that activation of the hydrolases AmiA and AmiB is most important when MreB is disrupted.

As might be expected, the *envC* and *amiAB* deletions result in similar phenotypes of elongated and chained cells (Figure 2a) (Uehara et al., 2010). As both strains are sensitive to A22 we examined all the strains under the microscope when grown with and without A22 to determine what effect A22 has on cell shape. All cells were grown in LB for 2 h before A22 (10 μg/ml) was added and cells were allowed to grow for another 2 h. An LB only control was allowed to grow for 4 h in total. As expected, WT cells become spherical upon A22 treatment. A similar change in shape was observed for all strains (Fig. 2AB). The *amiAB* double deletion exhibits a similar phenotype to the *envC* mutant both with and without A22. The *amiAC* deletion strain exhibits a more pronounced chaining phenotype than the *amiAB* mutant when grown in LB (Figure 2a) (Mueller et al., 2021). This suggests that the increased sensitivity of the *envC* and *amiAB* mutants to A22 is not due to those cells being chained, as the *amiAC* strain is more resistant to A22 than either of those strains and forms longer chains (Figure 1b and 2a).

2.3 | Loss of amidase activity increases sensitivity to envelope targeting antibiotics

It is possible that the above phenotypes are due to a general mechanism increasing cell permeability rather than a specific MreB mechanism. It has been shown that deletion of *envC* causes an increase in permeability as seen by sensitivity to vancomycin and bacitracin, cell wall targeting antibiotics that normally do not pass through the outer membrane (Heidrich et al., 2002). This permeability is thought to work through the amidases as mutants in different amidases also lead to increases in cell permeability (Heidrich et al., 2002; Ize et al., 2003; Yakhnina et al., 2015).

To test if the *envC* mutant is more sensitive to all antibiotics, we tested for growth in a low and high amount of ampicillin, tetracycline, and chloramphenicol. The low amount is below the inhibitory concentration for WT cells and the high amount shows a significant decrease in grow of WT cells. The *envC* mutant only displays an increased sensitivity to ampicillin, the cell well targeting drug, but not the ribosomal targeting antibiotics (Figure S2a). These data suggest that loss of amidase activity leads to increased sensitivity to envelope targeting antibiotics in *E. coli*, but not a generalized sensitivity to all antibiotics; therefore, we do not believe cell permeability is the cause of the increased sensitivity.

2.4 | Disruption of MreB reduces chaining caused by loss of amidase activity

We characterized the effects of A22 on each of the amidase mutants by measuring the change in rod shape and size of the cells. Using the metric, coefficient of variation of intracellular diameter deviation (IDD), we can measure the "rodness" of cells (Bratton et al., 2018; Grinnell et al., 2022; Morgenstein et al., 2015). A centerline is drawn through the long axis of the cell and the diameter is measured across the cell body. The change in the standard deviation of these diameters is used to determine "rodness", as a sphere will have a greater standard deviation than a rod. All strains tested become spherical upon A22 treatment (increased IDD) (Fig. 2AB). As cell length will affect the IDD value (longer cells reduce the influence of the poles) and *envC* cells are longer (Figure S3) we did not attempt to statistically compare IDD values across strains. Not only do all cells treated with A22 become spherical, but there is a concurrent increase in cell area (Figure 2c). Interestingly, the

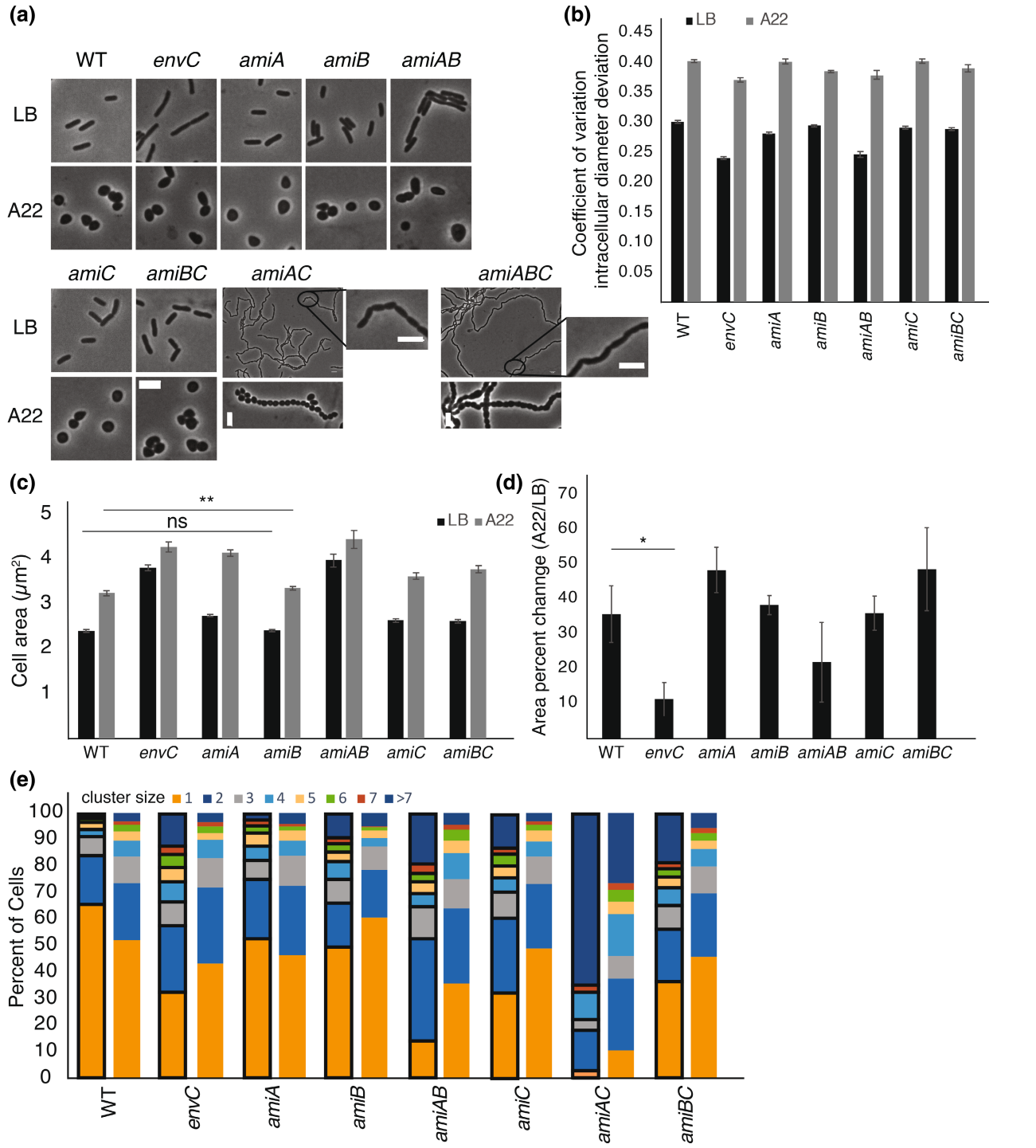

FIGURE 2 Cell shape characteristics of mutants involved in cell separation with and without A22. (a) Phase contrast images of cells grown in LB for 4 h or LB for 2 h and then A22 (10 μg/ml) for 2 h. Scale bar = 4 μm. (b–d) Data is pooled from three independent experiments. Only individual cells were counted, and chains of cells were ignored in the analysis. Cells were grown for 2 h in LB before the addition of A22 for 2 h. (b) Coefficient of variation diameter deviation is a metric to measure how 'rodlike' cells are. The higher the number the less rod and more spherical a cell is. (c) Cell area measurements of cells grown in A. All statistical comparisons were made between WT LB and mutants LB or WT A22 and mutants A22 and have a p value <0.001 unless noted. $^{**}p < 0.01$. See table S3 for number of cells. (d) Percent change of cell area between cells grown in LB or with A22. Error bars are standard deviation from three independent experiments. All comparison are to WT and not significant unless noted. $^{*}p < 0.5$. (b–D) error bars are 95% CI. (e) Cell cluster sizes were counted from images of cells grown in LB or LB + A22 as in A. Data for LB cells are bordered in black (left for each pair). Data is pooled from experiments performed three times. >100 clusters were counted for each strain in each replicate.

increase in area upon A22 treatment is smaller in Δ*envC* cells than WT cells (Figure 2d).

It is well established that *envC* and amidase mutants form chains of cells when grown in LB (Bernhardt & de Boer, 2004; Hara et al., 2002; Mueller et al., 2021; Uehara et al., 2009). This chaining phenotype is reduced when cells are treated with A22 (Figure 2e). After A22 treatment, all strains except for the Δ*amiAC* mutant have ~70% of their cells alone or in pairs, with a small percentage of cells found in clusters of larger groups. However, the *amiAC* mutant has ~30% of its cells found in large (>7 cells) clusters (Figure 2e). While this is a much larger percentage than the WT or *envC* mutants, it is a reduction from the *amiAC* mutant grown in LB. These data suggest some crosstalk between MreB and the cell separation machinery as the disruption of MreB with A22 leads to a reduction in cell chaining.

It is possible that the decreased growth caused by the addition of A22 leads to reduced chaining by aiding in cell separation. To determine if growth rate effects cell chaining, we grew WT, Δ*envC*, Δ*amiAB*, and Δ*amiAC* mutants at 30°C to slow their growth rate and then measured cell chaining. We found that lower temperatures increased rather than decreased chaining for amidase deficient mutants (Figure S4). When grown at 37°C the Δ*envC* and Δ*amiAB* mutants have ~70% of their clusters in groups of 1–2 and only 3% or 4.5% of clusters are greater than 7, while the *amiAC* mutant has 37.5% of clusters sized 1–2 and 26% >7 cells (Figure 2e); however, when grown at 30°C the percentage of cells in 1–2 sized clusters drops dramatically to 60 and 27% for the Δ*envC* and Δ*amiAB* strains while the Δ*amiAC* strain sees a drop to 8.5%. Similarly, the largest sized clusters (>7) increased to 9% and 27% for the Δ*envC* and Δ*amiAB* strains and 41% for the Δ*amiAC* strain. These results clearly show that reduced growth does not coorelate with less chaining; however, it is possible that there is an unknown temperature sensing mechanism at play.

2.5 | Suppressor mutations in the *envC* deletion strain can grow in A22

We have shown that an *envC* deletion is more sensitive to A22 treatment in an AmiAB dependent manner; however, it is still unclear why the loss of AmiAB function results in increased A22 sensitivity. The *envC* mutant does not grow in high levels of A22, whereas WT cells are able to grow (Figure 1). We performed a random suppressor screen, by plating the *envC* mutant on A22 plates to find mutants that restore growth. Colonies that grew on A22 plates were streaked onto fresh A22 plates before being grown in liquid cultures with A22, at 37°C. These experiments were performed independently three times. As a control of the acquisition of non-allele specific mutations that make the cells resistant to A22, we moved a known A22 resistant MreB point mutation ($MreB_{S14A}$) into the *envC* deletion (Bratton et al., 2018). This resistant *envC* strain is able to grow in A22 and has an elongated/chained phenotype when grown in LB, although the poles appear to taper (Figure 3 top). Any colony that grew throughout this selection process was tested for its A22 growth ratio in low and high levels of A22.

We classified the suppressor mutations into three categories based on A22 resistance. Group 1 consists of four mutants (#s 2, 3,

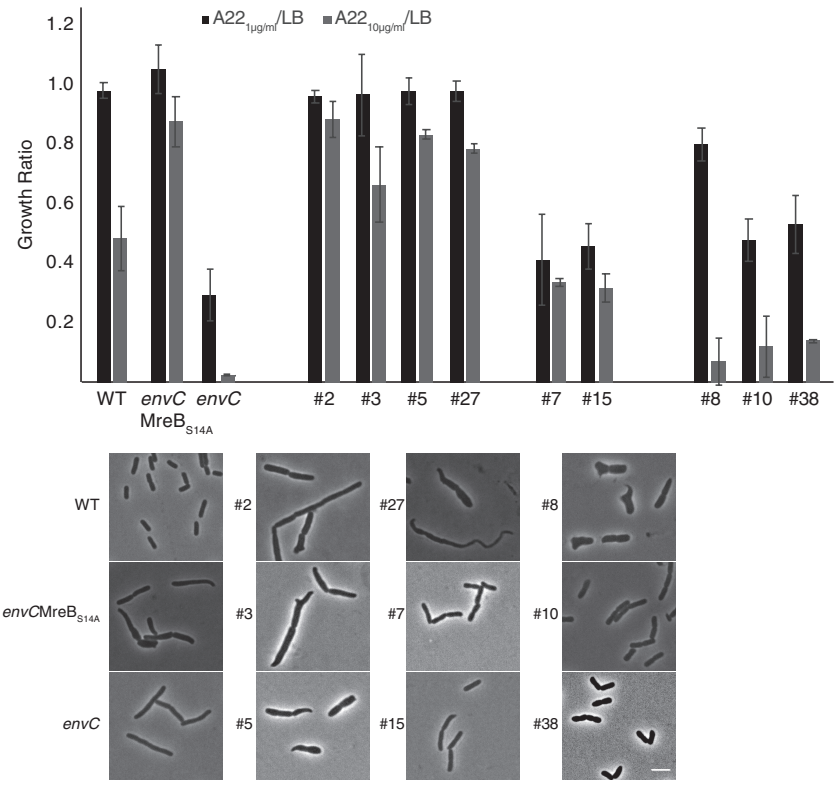

FIGURE 3 Suppressor screen for mutants of Δ*envC* cells that can grow in A22. Suppressors were selected with multiple rounds of growth on A22 10 μg/ml. Top- Cells are separated into four groups. The leftmost is a group of control strains, including WT, Δ*envC*, and Δ*envC* + an MreB point mutation resistant to A22 ($MreB_{S14A}$). Group 1 contains four strains with high levels of A22 resistance. Group 2 has two strains with increased growth in high levels of A22 and group 3 has three strains with high growth in low A22 and increased growth in high levels. Error bars are standard deviation from three independent experiments. Bottom-representative images of cells grown in LB medium. Scale bar = 4 μm.

5, 27) that display a high level of resistance, most similar to the WT or Δ*envCmreB*$_{S14A}$ strains. Group 2 mutants (#s 7, 15) do not show much change in low levels of A22 but are able to grow in A22 10 μg/ml, unlike the parental *envC* deletion. Group 3 (#s 8, 10, 38) consists of mutants that grow very well in low A22 but only show a small increase in growth at higher A22 levels (Figure 3 top).

To help determine the function of these suppressor mutations we imaged all strains in LB to compare their cell shapes with WT, Δ*envC*, and Δ*envCmreB*$_{S14A}$ stains, and sequenced *mreB*. Five of the nine suppressors have point mutations in *mreB* (Table S2). Interestingly, all group 1 mutants have point mutations in *mreB*, although mutants #5 and #27 have unique shapes that deviate from the shape of the *envC* mutant, suggesting that these mutations have a function distinct from generic A22 resistance (Figure 3 bottom). The other *mreB* point mutant is in group 3 (#8) and results in loss of the elongation and chaining seen when *envC* is removed. This mutant and mutant #27 have a missense mutation in residues close to each other yet have different A22 resistance profiles and different cell shapes (Figure 3, Table S2), suggesting that changes in one region of MreB can have different phenotypes both for A22 resistance and cell shape.

We performed whole-genome sequencing on all mutants without an *mreB* mutation (#s 7, 15, 10, 38) and the three mutants with *mreB* point mutations with shapes that deviate from the MreB$_{S14A}$ control (#s 5, 27) or are in a different resistance group (#8) (Table S2). Due to their similar shape and resistance profile to Δ*envCmreB*$_{S14A}$, we did not perform whole-genome sequencing on #s 2 and 3.

Both strains in group 2 have an insertion in *ptsI*, encoding for enzyme 1 of the PTS (Kundig et al., 1964). The three mutants in group 3 have no mutation in common. Mutant #8 has an *mreB* point mutation, while the sequencing of mutant #38 did not reveal any changes. Mutant #10 has a ~13 kb deletion of many genes involved in chemotaxis and flagella rotation. Due to known connections between metabolism and cell size we will focus on the role of *ptsI* on A22 resistance (Barton et al., 2021; Irnov et al., 2017; Vadia et al., 2017; Westfall & Levin, 2018). It is of note that mutants #3 and #5 have mutations in adjacent residues of MreB which are predicted to be in the A22 binding pocket, yet produce different cell shapes (Table S2) (van den Ent et al., 2001). As this screen was not saturating it is possible that mutations in other genes can suppress Δ*envC* growth on A22.

2.6 | Loss of functional PtsI increases resistance to cell wall targeting antibiotics

ptsI encodes for enzyme 1 in the PTS, which is used to transport and phosphorylate sugars, such as glucose, as they enter the cell (Deutscher et al., 2006). As all the described experiments were performed in LB without the addition of any sugar, it is surprising to find suppressor mutations in *ptsI*. The suppressors have the same two base pair insertion in the gene (Table S2); therefore, we tested whether a deletion of *ptsI* also increases A22 resistance. Deletion of *ptsI* in a WT background leads to increased resistance to high levels of A22 and can recapitulate the suppressor phenotype in an Δ*envC* background (Figure 4a), supporting the hypothesis that the original suppressor phenotype came about from the loss of PtsI function. This also suggests that loss of *ptsI* acts a general suppressor of A22 and is not specific to the Δ*envC* background.

PtsI is the first protein in the PTS which transfers a phosphate from phosphoenolpyruvate (PEP) and shuttles it to enzyme 2 of the PTS, where it can be added to sugars upon entry into the cell. PtsI is phosphorylated on residue H189. To further confirm the role of PtsI in A22 resistance we complemented the *ptsI* and *envCptsI* deletion strains with either a WT allele of PtsI or an allele that in unable to be phosphorylated (PtsI$_{H189A}$) (Dimitrova et al., 2002; Lopian et al., 2010). If PtsI phosphorylation is linked to its role in A22 sensitivity than the H189A mutant should mimic the deletion strain and provide increased resistance to A22. We found that complementation with the WT allele makes both the *ptsI* and *envCptsI* deletion strains more sensitive to A22 than when complemented with the nonphosphorylatable allele (Figure S5), supporting our hypothesis that the loss of PtsI activity increases the resistance of cells to disruption of MreB.

Slow growth has been shown to suppress the effects of elongasome targeting antibiotics (Bendezú & de Boer, 2008). However, slow growth is not sufficient for A22 resistance as the *envC* mutant has a growth defect (Figure S1) and the *tusE* mutant has a severe growth defect, yet both are more sensitive, not resistant, to A22 (Grinnell et al., 2022). To test the role of growth rate on the sensivity of the *envC* mutant we grew WT and Δ*envC* cells at 30°C with and without A22$_{10}$. Because of the slow growth caused by the lower temperature, we grew cells for 8 h instead of 6 h as in previous experiments. WT cells appear to be more sensitive to A22$_{10}$ at 30°C with a growth ratio of 0.14 (30°C) vs ~0.5 (37°C). Δ*envC* cells are stil more sensitive to A22 than WT cells but do grow in A22$_{10}$ at 30°C (growth ratio 0.12), unlike at 37°C. While slow growth due to temperature may aid the *envC* mutant in A22 growth, it harms WT cells and suggests that the effects of deleting *ptsI* are not through slow growth.

One of the common mechanisms for suppression of the lethality of MreB disruption is the upregulation of the *ftsZAQ* operon. It is possible that deletion of *ptsI* leads to increased levels of transcription from the *ftsZ* operon, providing resistance to A22. We transduced a functional fluorescent translational fusion fo *ftsZ* into the native site of the chromosome as the sole copy of *ftsZ* in the cell (Barton et al., 2021). A *ptsI* deletion strain expressing this construct is still smaller than WT cells (Figure S6). These strains allowed us to use fluorescence intensity to determine if there are changes in FtsZ levels caused by deleting *ptsI*. We found similar albeit slightly lower levels of FtsZ-GFP in the Δ*ptsI* strain when accounting for cell size ($3.88 \times 10^5 \pm 2.77 \times 10^5$ versus $3.03 \times 10^5 \pm 2.25 \times 10^5$ AU/pixel) suggesting that the suppressive effect of *ptsI* deletion is not due to increases in *ftsZ* levels. We also noticed that cells deleted for *ptsI* are more likely to lack an FtsZ structure. Although this was rare in both WT (4.5%) and Δ*ptsI* (8.5%) cells, the lack of FtsZ structures would not account for smaller cells (Figure S6 white arrows).

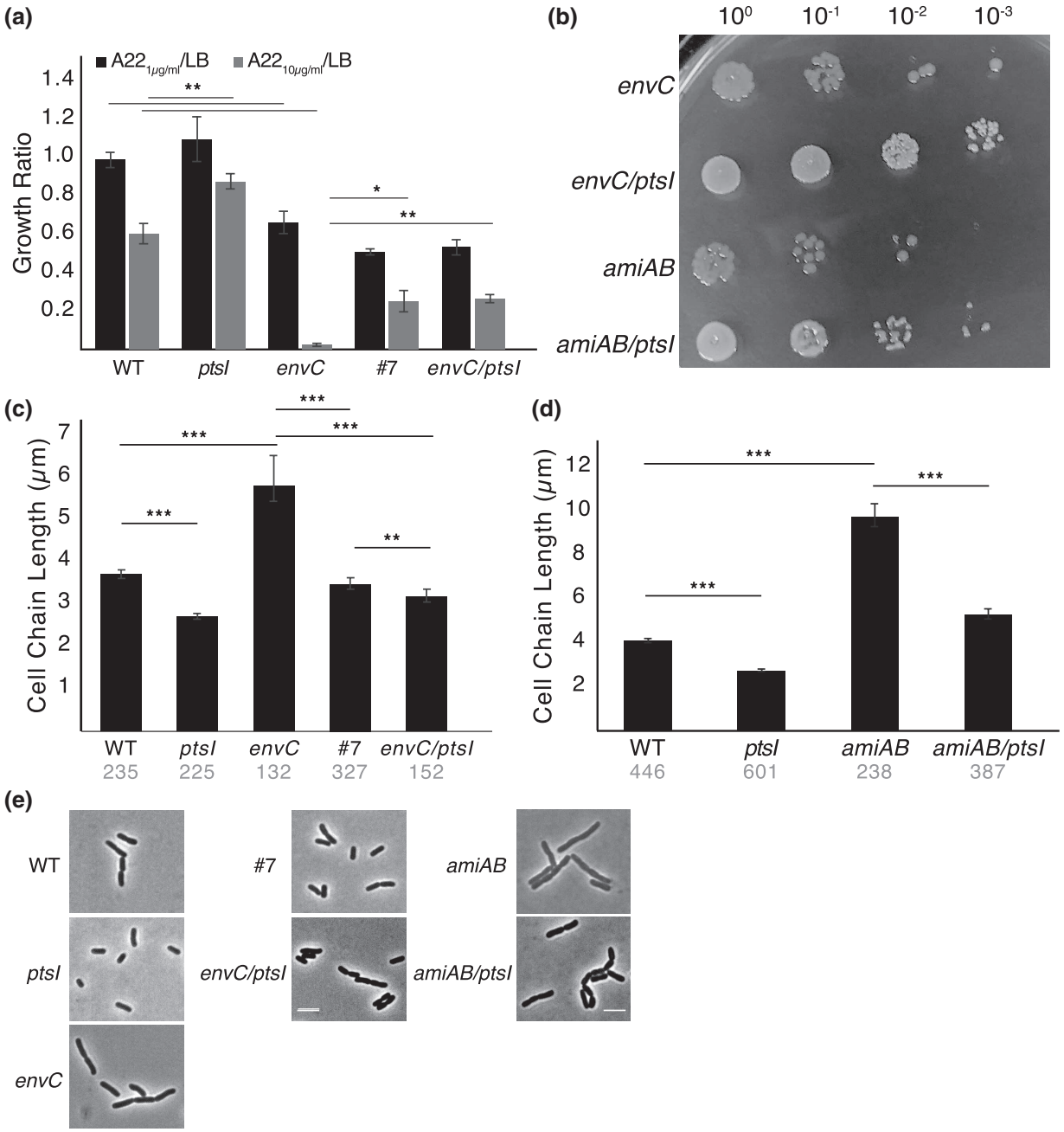

FIGURE 4 Deletion of *ptsI* suppresses both A22 and cell elongation phenotypes of Δ*envC* cells. (a) Average growth ratio from three experiments of cells grown in LB or LB + A22. Error bars are standard deviation. $^{*}p < 0.05$, $^{**}p < 0.01$. (b) Spot assays of indicated strains grown in LB + A22 (10 μg/ml) for 6 h before serial dilution and plating on LB. Plates were incubated overnight at 37°C. (c and d) Cell length of WT and indicated mutant cells. Cells in chains were included to capture the effect of chaining in different backgrounds. Cells were pooled from three experiments with total number of cells included in gray. Error bars are 95% CI and scale bar = 4 μm. $^{**}p < 0.01$, $^{***}p < 0.001$.

In addition to A22, we found that Δ*envC* cells are sensitive to ampicillin. To determine if the deletion of *ptsI* is specific to A22 treatment or more general cell wall stresses, we tested the sensitivity of the *envCptsI* double mutant in ampicillin and found that the loss of *ptsI* is able to suppress the sensitivity to ampicillin at high concentrations, similar to that seen with A22 (Figure S2b) suggesting that the lack of PtsI has general effect against cell wall targeting compounds.

2.7 | Deletion of *ptsI* causes A22 resistance by two mechanisms

We have shown that the sensitivity to A22 seen in *envC* cells works through *amiAB* (Figure 1b); therefore, we tested if deletion of *ptsI* would also suppress the A22 sensitivity in an *amiAB* background. Due to the severe growth defects of both the *envC* and *amiAB* mutants in $A22_{10}$, O.D. readings are not sensitive enough to accurately

measure differences in growth. Therefore, we serially diluted the *envC*, *envC/ptsI*, *amiAB*, and *amiAB/ptsI* mutants on LB plates after growth in $A22_{10}$ for 6 h. As expected, we saw a 10-100X fold increase in growth when *ptsI* is deleted in the *envC* background (Figure 4b). While deletion of *ptsI* in an *amiAB* background leads to increase growth over the *amiAB* deletion alone, the *amiAB/ptsI* mutant does not grow to the same level as the *envC/ptsI* strain (Figure 4b). This suggests that there are two possible mechanisms for the suppressive effect of losing PtsI: one works through AmiA and/or AmiB, and the second is independent of the amidases. This datum also suggests that the loss of PtsI does not change membrane permeability, as we would expect all strains that have increased A22 sensitivity to become equally resistant if permeability of A22 was affected.

2.8 | Loss of *ptsI* results in cell size changes

One of the initial observations of an *envC* mutant was that it forms elongated and chained cells (Figures 3a and 4c, Figure S3) (Bernhardt & de Boer, 2004). Because deletion of *ptsI* suppresses the A22 sensitivity phenotype through AmiA/AmiB, we asked whether cell size is also affected. Cells were grown in LB without additional sugar, to mid log phase and imaged. To account for the chaining effect of the *envC* mutant, we measured both individual and chained cells. As expected, Δ*envC* cells are longer than WT; interestingly, the lack of *ptsI* reduces the cell length of WT cells and Δ*envC* cells (Figure 4c). Since deletion of *ptsI* is only able to provide partial resistance to *amiAB* cells, we examined if deletion of *ptsI* would reduce the cell size of the *amiAB* mutant. Deletion of *ptsI* is able to reduce cell length in the absence of *amiAB* (Figure 4d). These results show that loss of *ptsI* can suppress the cell length phenotype resulting from the loss of *envC* or *amiAB*, suggesting that the role of PtsI in A22 resistance cannot be separated from its role in cell size regulation.

3 | DISCUSSION

MreB is a highly conserved protein essential for the regulation of rod shape and viability, making it a potentially good target for antibiotic development (Bendezú & de Boer, 2008; Shi et al., 2018). While we have previously reported on conditions that help cells grow without MreB, there is little known about how cells can become hypersensitive to the disruption of MreB (Barton et al., 2021; Grinnell et al., 2022). Here, we performed a screen of the Keio collection to identify gene deletions that lead to the inhibition of growth in sublethal levels of A22, an MreB depolymerizing agent. Five strains were found to have increased sensitivity to A22, one of which, *envC*, is involved in cell division (Figure 1a).

There are two distinct cell wall synthesis complexes in rod-shaped bacteria, the MreB-regulated elongasome controlling cell elongation and growth, and the FtsZ-regulated divisome controlling cell division. If and how these two systems talk with each other is underexplored. While it is well established that MreB localizes to the Z-ring during division in *Caulobacter crescentus*, it is more controversial in *E. coli* (Figge et al., 2004; Yakhnina & Gitai, 2012). While our lab and others have not been able to see an enrichment of MreB at the division site when using a functional fluorescent sandwich fusion of MreB as the only copy in the cell, others have reported that N-terminal fusions to MreB and the MreB interaction partner, RodZ, localize to the midcell, and interact with FtsZ (Fenton & Gerdes, 2013; van der Ploeg et al., 2013; Yoshii et al., 2019). This putative interaction between MreB and other elongasome partners with the division machinery suggests that crosstalk between these two cell wall synthesis complexes is important. This study reinforces that there is some crosstalk between these two systems as loss of *envC* (divisome) makes cells more sensitive to disruption of MreB (elongasome) with A22.

The "adder-model" of cell size regulation says that rather than reach a critical size before dividing, cells add a constant volume before dividing (Campos et al., 2014; Taheri-Araghi et al., 2015). It would reason that there is coordination between lateral wall synthesis controlled by MreB and cell division. Why this system would work at the level of cell separation after division is unclear, but it may suggest the role of proteins upstream or downstream of EnvC, such as FtsEX or FtsN (Bernhardt & de Boer, 2004; Peters et al., 2011).

3.1 | Loss of *amiA* and *amiB* phenocopy *envC*'s A22 sensitivity

EnvC activates two cell wall hydrolases, AmiA and AmiB, needed to separate daughter cells after division has occurred. To determine if the sensitivity of the *envC* deletion is due to a secondary role of EnvC or its role in activating AmiA and AmiB, we deleted both proteins alone and together. The double *amiAB* deletion was even more sensitive to A22 than the *envC* deletion (Figure 1). This is most likely due to latent activity of either enzyme in the *envC* deletion that is absent when the proteins are deleted. It will be interesting in future work to determine if AmiA and/or AmiB have a secondary role in the cell that when absent leads to cells being more sensitive to changes in MreB polymerization.

The activity of the amidases during cell division produces denuded glycan chains (missing peptide side chains) which signal to activate FtsN (Gerding et al., 2009; Ursinus et al., 2004). When active, FtsN activates PBP1B at the division site (Boes et al., 2019). PBP1B mutants are sensitive to A22, and PBP1B is necessary to overcome the loss of the elongation machinery (Barton et al., 2021; García del Portillo et al., 1989; Grinnell et al., 2022). One possible reason for the increased sensitivity of an *envC* mutant to A22 is a lowering of the presence of denuded glycans leading to less active FtsN and therefore less active PBP1B, mimicking a PBP1B deletion. Without a highly active PBP1B the cell would not be able to overcome the loss of the elongasome. This model relies on regulation of PBP1B activity rather than a direct interaction between MreB and EnvC or the amidases.

Alternatively, if MreB does interact with EnvC or the amidases, one must ask how. In the elongasome we have proposed that the

cytoplasmic MreB is linked to cell wall synthesis through RodZ (Morgenstein et al., 2015). As RodZ has been shown to interact with FtsZ and therefore be at the division site it could act similarly to link MreB with the periplasmic domains of EnvC or AmiAB (Yoshii et al., 2019). FtsEX is a transmembrane protein that helps to regulate amidase activity by modulating EnvC activity (Yang et al., 2011). MreB could interact with FtsEX to help coordinate division and elongation through EnvC and therefore amidase activity.

It has been proposed that elongation and division compete for cell wall precursors and are antagonistic processes with each other (Begg & Donachie, 1985; Canepari et al., 1984; Truong et al., 2020). An alternative explanation for the increased A22 sensitivity in an *envC* mutant is that the there are changes to the geometry of the cell poles, leading to less positive Gaussian curvature at the poles that have not fully separated. MreB is known to avoid areas of high Gaussian curvature, therefore, changes to the polar architecture might lead to changes in MreB distribution (Bratton et al., 2018). If these changes increase the activity of MreB to help cells with separation problems grow than the addition of A22 would be detrimental.

3.2 | A22 sensitivity caused by loss of *cpxR* is not due to changes in amidase expression

The CpxR/CpxA two-component system has been shown to positively regulate the expression of both *amiA* and *amiC* (Weatherspoon-Griffin et al., 2011). As a mutant of *cpxR* was found to be more sensitive to A22 (Figure 1a) and an *amiAC* double mutant is more sensitive to A22 (Figure 1b) we asked if the sensitivity of the Δ*cpxR* deletion strain was due to loss of *amiA* and/or *amiC* expression. We cloned *amiA*, *amiB*, and *amiC* into the vector pTrc99A under the control of a leaky lac promoter and attempted to suppress the A22 sensitivity of the Δ*cpxR* strain through ectopic expression of any of the amidases. While there does appear to be some effect of the empty vector on A22 sensitivity, expression of any amidase was unable to restore growth in A22 to WT levels in the *cpxR* mutant (Figure S7). This suggests a distinct mechanism of A22 sensitivity in the Δ*cpxR* strain.

3.3 | Point mutations in *mreB* suppress effects of *envC*

In order to further understand the connection between MreB and EnvC we performed an A22 resistance suppressor screen. Of the nine suppressor strains found in this screen, five have mutations in *mreB* leading to amino acid changes. Interestingly, while 4/5 of the *envCmreB* mutants have increased A22 resistance over WT cells, 3/5 have unique cell shapes in LB medium (Figure 3). Mutants #5 and #27 are both shorter than the *envC* parent strain with tapered tails and do not appear to chain. Furthermore, #3 and #5 have mutations in adjacent residues that are predicted to interact with ATP, yet cause different cell shapes (van den Ent et al., 2001). Molecular dynamic simulations suggest that ATP binding of the MreB monomer is necessary for polymerization and that polymerization induces structural changes in MreB leading to hydrolysis; therefore, we suggest that these two mutations may help stabilize ATP-binding leading to increased filamentation and A22 resistance (Colavin et al., 2014). Alternatively, these mutations may decrease the exchange between ADP and ATP, stabilizing filaments and leading to A22 resistance. The nucleotide-bound state of MreB polymers may also affect membrane binding or protein interactions, as seen with eukaryotic actin (dos Remedios et al., 2003; Dye et al., 2011).

Residues 72 (#8) and 79 (#27) are near each other on the MreB protein but are not predicted to have a structural role in filamentation and lead to different A22 resistance profiles and cell shapes (Figure S7). These residues may represent an MreB-protein interaction site. It will be interesting to study the effects of these MreB mutations in a background with *envC* to see if cell shape effects are due to the loss of *envC*.

3.4 | PtsI regulates cell size even without excess sugars

Cells can sense their metabolic environment and adjust their size accordingly. The fact that cells grow larger in rich medium and smaller in nutrient poor medium is termed the "Growth Law" (Schaechter et al., 1958). One mechanism for connecting nutrient levels with cells size links the inhibition of FtsZ with UDP-glucose levels (Hill et al., 2013; Weart et al., 2007). Our experiments reveal that deletion of *ptsI* results in shorter cells in WT, Δ*envC*, and Δ*amiAB* backgrounds (Figure 4c). Interestingly, these cells were grown in LB medium without the addition of sugar. As the PTS is involved in sugar uptake, it is surprising to find such a dramatic change in cell length in these conditions.

Lack of PtsI will affect the PEP: pyruvate ratio of the cell (Long et al., 2017; Waygood & Steeves, 1980). We have previously proposed that increased pyruvate levels in cells can activate gluconeogenesis and increase the levels of cell wall precursors providing cells with increased tolerance to A22 (Barton et al., 2021). In *Bacillus subtilis*, deletion of pyruvate kinase (*pyk*) effects Z-ring formation (Monahan et al., 2014). We propose that deletion of *ptsI* results in a change in the PEP: pyruvate ratio in the cell, resulting in increased resistance to A22 and changes in cell size. However, it is also possible that changes in the PTS affect cAMP levels, which has been shown to regulate cell shape (Westfall & Levin, 2018).

4 | EXPERIMENTAL PROCEDURES

4.1 | Bacterial growth

Bacteria were grown using standard laboratory conditions. Cultures were grown overnight in LB medium (10 g/L NaCl, 10 g/L

tryptone, 5 g/L yeast extract) and subcultured in the morning 1:1000 and grown to exponential phase ($O.D._{600}$ 0.2–0.5) at 37°C in a shaking incubator. Keio collection mutant alleles were moved in MG1655 using P1 transduction. Phage were propagated in a WT MG1655 strain before being grown with PCR verified mutants from the Keio collection. Tranducing phage were then grown on MG1655 and transductants were selected on kanamycin (30 μg/ml) and confirmed by PCR. See Table S1 for a list of strains used in this study.

4.2 | Cloning

Genes for insertion into plasmids were cloned via PCR amplication followed by restriction enzyme digestion and T4 ligation. *envC* was cloned into Pbad33 by the addition of SacI and HindIII restriction sites at the ends of the gene using PCR. The native ribosome binding site was used. *amiA*, *amiB*, and *amiC* were cloned into Ptrc99A through the addition of XbaI and HindIII sites by PCR and included the native RBS.

4.3 | Growth ratios

Overnight cultures of cells were subcultured 1:1000 into media with 1 or 10 μg/ml, or no A22. Cultures were grown shaking at 37°C for 6 h, unless indicated, before measuring the $O.D._{600}$. Growth ratios were determined for each strain comparing the A22 cultures to the no drug culture. Error bars were determined by taking the standard deviation of the growth ratio across multiple experiments.

4.4 | Spot assay

Equal amounts of cells based on $O.D._{600}$ readings from overnight cultures were added to fresh LB media with A22 (10 μg/ml). Cultures were grown shaking at 37°C for 6 h before serial dilutions were made. 5 μl drops for each strain from each dilution were plated onto an LB plate and incubated overnight at 37°C.

4.5 | Suppressor screen

A22 suppressors of the Δ*envC* mutant were isolated by growing Δ*envC* cells overnight in LB media lacking A22. Cells were plated on LB + A22 (10 μg/ml) and incubated for 16 h at 37°C. Colonies were streaked onto fresh A22 plates and incubated for 16 h at 37°C. Colonies were then grown in liquid A22 media for 16 h.

Mutants that grew in liquid media were subjected to growth ratio analysis in A22 1 and 10 μg/ml and imaged from exponential phase in LB medium. *mreB* was PCR amplified and sequenced before strains were sent to MiGS for whole-genome Illumina sequencing. Both the Δ*envC* parent and suppressors were sequenced. Indicated mutations are the only differences. Variants were found using breseq on census/mixed base mode (Deatherage & Barrick, 2014). The consensus mutation E-value cutoff and polymorphism E-cutoff was set to 10 with a frequency cutoff of 0.8 and a polymorphism frequency cutoff of 0.2.

4.6 | Microscopy

For all imaging, cells were grown at 37°C in LB medium. Imaging was done on 1% M63-glucose agarose pads at room temperature. Phase contrast and fluorescent images were collected on a Nikon Ni-E epifluorescent microscope equipped with a 100X/1.45 NA objective (Nikon), Zyla 4.2 plus cooled sCMOS camera (Andor), and NIS Elements software (Nikon).

Cell area and IDD were calculated using the matlab software Morphometrics (Ursell et al., 2017), and custom software as described previously (Morgenstein et al., 2015). Only single non-diving cells were used for analysis unless stated otherwise.

4.7 | MreB mutation modeling

MreB amino acid changes were modeled using Swiss model server (SWISS-MODEL (expasy.org)) using *Caulobacter crescentus* MreB (4czg.1.pdb) (https://swissmodel.expasy.org/templates/4czg.1) as a template. The changes were mapped using PymoL Version 2.5.2.

AUTHOR CONTRIBUTIONS

Ryan Sloan: Conceptualization; investigation. **Jacob Surber:** Formal analysis; investigation. **Emma J. Roy:** Investigation. **Ethan Hartig:** Investigation. **Randy M. Morgenstein:** Conceptualization; data curation; formal analysis; funding acquisition; investigation; project administration; supervision; writing – original draft; writing – review and editing.

ACKNOWLEDGMENTS

Thanks to Dr. Oma Amster-Choderl for PtsI strains. Thank you to Dr. Elizabeth Ohneck for careful reading of the manuscript. This work was funded by NIH 1R15GM129636-01A1.

CONFLICT OF INTEREST

The authors declare no conflict of interest.

DATA AVAILABILITY STATEMENT

The data that support the findings of this study are available from the corresponding author upon reasonable request.

ETHICS STATEMENT

No human or animal subjects were used in this study.

ORCID

Randy M. Morgenstein https://orcid.org/0000-0003-0749-6830

REFERENCES

Alyahya, S.A., Alexander, R., Costa, T., Henriques, A.O., Emonet, T. & Jacobs-Wagner, C. (2009) RodZ, a component of the bacterial core morphogenic apparatus. *Proceedings of the National Academy of Sciences of the United States of America*, *106*(4), 1239–1244. https://doi.org/10.1073/pnas.0810794106

Baba, T., Ara, T., Hasegawa, M., Takai, Y., Okumura, Y., Baba, M. et al. (2006) Construction of *Escherichia coli* K-12 in-frame, single-gene knockout mutants: the keio collection. *Molecular Systems Biology*, *2*, 2006.0008. https://doi.org/10.1038/msb4100050

Barton, B., Grinnell, A. & Morgenstein, R.M. (2021) Disruption of the MreB elongasome is overcome by mutations in the tricarboxylic acid cycle. *Frontiers in Microbiology*, *12*, 664281. https://doi.org/10.3389/fmicb.2021.664281

Bean, G.J., Flickinger, S.T., Westler, W.M., McCully, M.E., Sept, D., Weibel, D.B. et al. (2009) A22 disrupts the bacterial actin cytoskeleton by directly binding and inducing a low-affinity state in MreB. *Biochemistry*, *48*(22), 4852–4857. https://doi.org/10.1021/bi900014d

Begg, K.J. & Donachie, W.D. (1985) Cell shape and division in *Escherichia coli*: experiments with shape and division mutants. *Journal of Bacteriology*, *163*(2), 615–622.

Bendezú, F.O. & de Boer, P.A.J. (2008) Conditional lethality, division defects, membrane involution, and endocytosis in *mre* and *mrd* shape mutants of *Escherichia coli*. *Journal of Bacteriology*, *190*(5), 1792–1811. https://doi.org/10.1128/jb.01322-07

Bendezu, F.O., Hale, C.A., Bernhardt, T.G. & de Boer, P.A.J. (2009) RodZ (YfgA) is required for proper assembly of the MreB actin cytoskeleton and cell shape in *E. coli*. *The EMBO Journal*, *28*(3), 193–204.

Bernhardt, T.G. & de Boer, P.A. (2004) Screening for synthetic lethal mutants in *Escherichia coli* and identification of EnvC (YibP) as a periplasmic septal ring factor with murein hydrolase activity. *Molecular Microbiology*, *52*(5), 1255–1269. https://doi.org/10.1111/j.1365-2958.2004.04063.x

Billings, G., Ouzounov, N., Ursell, T., Desmarais, S.M., Shaevitz, J., Gitai, Z. et al. (2014) De novo morphogenesis in L-forms via geometric control of cell growth. *Molecular Microbiology*, *93*(5), 883–896. https://doi.org/10.1111/mmi.12703

Boes, A., Olatunji, S., Breukink, E. & Terrak, M. (2019) Regulation of the peptidoglycan polymerase activity of PBP1b by antagonist actions of the core divisome proteins FtsBLQ and FtsN. *MBio*, *10*(1), e01912-18. https://doi.org/10.1128/mBio.01912-18

Bratton, B.P., Shaevitz, J.W., Gitai, Z. & Morgenstein, R.M. (2018) MreB polymers and curvature localization are enhanced by RodZ and predict *E. coli's* cylindrical uniformity. *Nature Communications*, *9*(1), 2797. https://doi.org/10.1038/s41467-018-05186-5

Campos, M., Surovtsev, I.V., Kato, S., Paintdakhi, A., Beltran, B., Ebmeier, S.E. et al. (2014) A constant size extension drives bacterial cell size homeostasis. *Cell*, *159*(6), 1433–1446. https://doi.org/10.1016/j.cell.2014.11.022

Canepari, P., Botta, G. & Satta, G. (1984) Inhibition of lateral wall elongation by mecillinam stimulates cell division in certain cell division conditional mutants of *Escherichia coli*. *Journal of Bacteriology*, *157*(1), 130–133. https://doi.org/10.1128/jb.157.1.130-133.1984

Cho, H., Uehara, T. & Bernhardt, T.G. (2014) Beta-lactam antibiotics induce a lethal malfunctioning of the bacterial cell wall synthesis machinery. *Cell*, *159*(6), 1300–1311.

Cho, H., Wivagg, C.N., Kapoor, M., Barry, Z., Rohs, P.D.A., Suh, H. et al. (2016) Bacterial cell wall biogenesis is mediated by SEDS and PBP polymerase families functioning semi-autonomously. *Nature Microbiology*, *1*, 16172.

Colavin, A., Hsin, J. & Huang, K.C. (2014) Effects of polymerization and nucleotide identity on the conformational dynamics of the bacterial actin homolog MreB. *Proceedings of the National Academy of Sciences of the United States of America*, *111*(9), 3585–3590. https://doi.org/10.1073/pnas.1317061111

Deatherage, D.E. & Barrick, J.E. (2014) Identification of mutations in laboratory-evolved microbes from next-generation sequencing data using breseq. *Methods in Molecular Biology*, *1151*, 165–188. https://doi.org/10.1007/978-1-4939-0554-6_12

Dempwolff, F., Reimold, C., Reth, M. & Graumann, P.L. (2011) *Bacillus subtilis* MreB orthologs self-organize into filamentous structures underneath the cell membrane in a heterologous cell system. *PLoS One*, *6*(11), e27035. https://doi.org/10.1371/journal.pone.0027035

Deutscher, J., Francke, C. & Postma, P.W. (2006) How phosphotransferase system-related protein phosphorylation regulates carbohydrate metabolism in bacteria. *Microbiology and Molecular Biology Reviews*, *70*(4), 939–1031. https://doi.org/10.1128/mmbr.00024-06

Dimitrova, M.N., Szczepanowski, R.H., Ruvinov, S.B., Peterkofsky, A. & Ginsburg, A. (2002) Interdomain interaction and substrate coupling effects on dimerization and conformational stability of enzyme I of the *Escherichia coli* phosphoenolpyruvate:sugar phosphotransferase System. *Biochemistry*, *41*(3), 906–913. https://doi.org/10.1021/bi011801x

dos Remedios, C.G., Chhabra, D., Kekic, M., Dedova, I.V., Tsubakihara, M., Berry, D.A. et al. (2003) Actin binding proteins: regulation of cytoskeletal microfilaments. *Physiological Reviews*, *83*(2), 433–473. https://doi.org/10.1152/physrev.00026.2002

Dye, N.A., Pincus, Z., Fisher, I.C., Shapiro, L. & Theriot, J.A. (2011) Mutations in the nucleotide binding pocket of MreB can alter cell curvature and polar morphology in *Caulobacter*. *Molecular Microbiology*, *81*(2), 368–394. https://doi.org/10.1111/j.1365-2958.2011.07698.x

Fenton, A.K. & Gerdes, K. (2013) Direct interaction of FtsZ and MreB is required for septum synthesis and cell division in *Escherichia coli*. *The EMBO Journal*, *32*(13), 1953–1965. https://doi.org/10.1038/emboj.2013.129

Figge, R.M., Divakaruni, A.V. & Gober, J.W. (2004) MreB, the cell shape-determining bacterial actin homologue, co-ordinates cell wall morphogenesis in *Caulobacter crescentus*. *Molecular Microbiology*, *51*(5), 1321–1332. https://doi.org/10.1111/j.1365-2958.2003.03936.x

García del Portillo, F., de Pedro, M.A., Joseleau-Petit, D. & D'Ari, R. (1989) Lytic response of *Escherichia coli* cells to inhibitors of penicillin-binding proteins 1a and 1b as a timed event related to cell division. *Journal of Bacteriology*, *171*(8), 4217–4221. https://doi.org/10.1128/jb.171.8.4217-4221.1989

Gerding, M.A., Liu, B., Bendezú, F.O., Hale, C.A., Bernhardt, T.G. & de Boer, P.A. (2009) Self-enhanced accumulation of FtsN at division sites and roles for other proteins with a SPOR domain (DamX, DedD, and RlpA) in *Escherichia coli* cell constriction. *Journal of Bacteriology*, *191*(24), 7383–7401. https://doi.org/10.1128/jb.00811-09

Gitai, Z., Dye, N. & Shapiro, L. (2004) An actin-like gene can determine cell polarity in bacteria. *Proceedings of the National Academy of Sciences of the United States of America*, *101*(23), 8643–8648. https://doi.org/10.1073/pnas.0402638101

Govindarajan, S. & Amster-Choder, O. (2017) The bacterial Sec system is required for the organization and function of the MreB cytoskeleton. *PLoS Genetics*, *13*(9), e1007017. https://doi.org/10.1371/journal.pgen.1007017

Grinnell, A., Sloan, R. & Morgenstein, R.M. (2022) Cell density-dependent antibiotic tolerance to inhibition of the elongation machinery requires fully functional PBP1B. *Communications Biology*, *5*(1), 107. https://doi.org/10.1038/s42003-022-03056-x

Hara, H., Narita, S., Karibian, D., Park, J.T., Yamamoto, Y. & Nishimura, Y. (2002) Identification and characterization of the *Escherichia coli envC* gene encoding a periplasmic coiled-coil protein with putative

peptidase activity. *FEMS Microbiology Letters*, *212*(2), 229–236. https://doi.org/10.1111/j.1574-6968.2002.tb11271.x

Heidrich, C., Ursinus, A., Berger, J., Schwarz, H. & Höltje, J.V. (2002) Effects of multiple deletions of murein hydrolases on viability, septum cleavage, and sensitivity to large toxic molecules in *Escherichia coli*. *Journal of Bacteriology*, *184*(22), 6093–6099. https://doi.org/10.1128/jb.184.22.6093-6099.2002

Hill, N.S., Buske, P.J., Shi, Y. & Levin, P.A. (2013) A moonlighting enzyme links *Escherichia coli* cell size with central metabolism. *PLoS Genetics*, *9*(7), e1003663. https://doi.org/10.1371/journal.pgen.1003663

Irnov, I., Wang, Z., Jannetty, N.D., Bustamante, J.A., Rhee, K.Y. & Jacobs-Wagner, C. (2017) Crosstalk between the tricarboxylic acid cycle and peptidoglycan synthesis in *Caulobacter crescentus* through the homeostatic control of α-ketoglutarate. *PLoS Genetics*, *13*(8), e1006978. https://doi.org/10.1371/journal.pgen.1006978

Ize, B., Stanley, N.R., Buchanan, G. & Palmer, T. (2003) Role of the *Escherichia coli* Tat pathway in outer membrane integrity. *Molecular Microbiology*, *48*(5), 1183–1193. https://doi.org/10.1046/j.1365-2958.2003.03504.x

Kruse, T., Bork-Jensen, J. & Gerdes, K. (2005) The morphogenetic MreBCD proteins of *Escherichia coli* form an essential membrane-bound complex. *Molecular Microbiology*, *55*(1), 78–89.

Kundig, W., Ghosh, S. & Roseman, S. (1964) Phosphate bound to histidine in a protein as an intermediate in a novel phospho-transferase system. *Proceedings of the National Academy of Sciences of the United States of America*, *52*(4), 1067–1074. https://doi.org/10.1073/pnas.52.4.1067

Lee, T.K., Tropini, C., Hsin, J., Desmarais, S.M., Ursell, T.S., Gong, E. et al. (2014) A dynamically assembled cell wall synthesis machinery buffers cell growth. *Proceedings of the National Academy of Sciences of the United States of America*, *111*(12), 4554–4559. https://doi.org/10.1073/pnas.1313826111

Long, C.P., Au, J., Sandoval, N.R., Gebreselassie, N.A. & Antoniewicz, M.R. (2017) Enzyme I facilitates reverse flux from pyruvate to phosphoenolpyruvate in *Escherichia coli*. *Nature Communications*, *8*, 14316. https://doi.org/10.1038/ncomms14316

Lopian, L., Elisha, Y., Nussbaum-Shochat, A. & Amster-Choder, O. (2010) Spatial and temporal organization of the *E. coli* PTS components. *The EMBO Journal*, *29*(21), 3630–3645. https://doi.org/10.1038/emboj.2010.240

Meeske, A.J., Riley, E.P., Robins, W.P., Uehara, T., Mekalanos, J.J., Kahne, D. et al. (2016) SEDS proteins are a widespread family of bacterial cell wall polymerases. *Nature*, *537*(7622), 634–638.

Monahan, L.G., Hajduk, I.V., Blaber, S.P., Charles, I.G. & Harry, E.J. (2014) Coordinating bacterial cell division with nutrient availability: a role for glycolysis. *MBio*, *5*(3), e00935-14. https://doi.org/10.1128/mBio.00935-14

Morgenstein, R.M., Bratton, B.P., Ouzounov, N., Nguyen, J.P., Shaevitz, J.W. & Gitai, Z. (2015) RodZ links MreB to cell wall synthesis to mediate MreB rotation and robust morphogenesis. *Proceedings of the National Academy of Sciences of the United States of America*, *112*, 12510–12515.

Mueller, E.A., Iken, A.G., Ali Öztürk, M., Winkle, M., Schmitz, M., Vollmer, W. et al. (2021) The active repertoire of *Escherichia coli* peptidoglycan amidases varies with physiochemical environment. *Molecular Microbiology*, *116*(1), 311–328. https://doi.org/10.1111/mmi.14711

Peters, N.T., Dinh, T. & Bernhardt, T.G. (2011) A Fail-safe mechanism in the septal ring assembly pathway generated by the sequential recruitment of cell separation amidases and their activators. *Journal of Bacteriology*, *193*(18), 4973–4983. https://doi.org/10.1128/jb.00316-11

Salje, J., van den Ent, F., de Boer, P. & Lowe, J. (2011) Direct membrane binding by bacterial actin MreB. *Molecular Cell*, *43*(3), 478–487.

Schaechter, M., Maaloe, O. & Kjeldgaard, N.O. (1958) Dependency on medium and temperature of cell size and chemical composition during balanced grown of *Salmonella typhimurium*. *Journal of General Microbiology*, *19*(3), 592–606. https://doi.org/10.1099/00221287-19-3-592

Shi, H., Bratton, B.P., Gitai, Z. & Huang, K.C. (2018) How to build a bacterial cell: MreB as the foreman of *E. coli* construction. *Cell*, *172*(6), 1294–1305.

Shiomi, D., Sakai, M. & Niki, H. (2008) Determination of bacterial rod shape by a novel cytoskeletal membrane protein. *The EMBO Journal*, *27*(23), 3081–3091. https://doi.org/10.1038/emboj.2008.234

Taheri-Araghi, S., Bradde, S., Sauls, J.T., Hill, N.S., Levin, P.A., Paulsson, J. et al. (2015) Cell-size control and homeostasis in bacteria. *Current Biology*, *25*(3), 385–391. https://doi.org/10.1016/j.cub.2014.12.009

Truong, T.T., Vettiger, A. & Bernhardt, T.G. (2020) Cell division is antagonized by the activity of peptidoglycan endopeptidases that promote cell elongation. *Molecular Microbiology*, *114*(6), 966–978. https://doi.org/10.1111/mmi.14587

Uehara, T., Dinh, T. & Bernhardt, T.G. (2009) LytM-domain factors are required for daughter cell separation and rapid ampicillin-induced lysis in *Escherichia coli*. *Journal of Bacteriology*, *191*(16), 5094–5107. https://doi.org/10.1128/jb.00505-09

Uehara, T., Parzych, K.R., Dinh, T. & Bernhardt, T.G. (2010) Daughter cell separation is controlled by cytokinetic ring-activated cell wall hydrolysis. *The EMBO Journal*, *29*(8), 1412–1422. https://doi.org/10.1038/emboj.2010.36

Ursell, T.S., Nguyen, J., Monds, R.D., Colavin, A., Billings, G., Ouzounov, N. et al. (2014) Rod-like bacterial shape is maintained by feedback between cell curvature and cytoskeletal localization. *Proceedings of the National Academy of Sciences of the United States of America*, *111*(11), E1025–E1034. https://doi.org/10.1073/pnas.1317174111

Ursell, T., Lee, T.K., Shiomi, D., Shi, H., Tropini, C., Monds, R.D. et al. (2017) Rapid, precise quantification of bacterial cellular dimensions across a genomic-scale knockout library. *BMC Biology*, *15*(1), 17. https://doi.org/10.1186/s12915-017-0348-8

Ursinus, A., van den Ent, F., Brechtel, S., de Pedro, M., Höltje, J.V., Löwe, J. et al. (2004) Murein (peptidoglycan) binding property of the essential cell division protein FtsN from *Escherichia coli*. *Journal of Bacteriology*, *186*(20), 6728–6737. https://doi.org/10.1128/jb.186.20.6728-6737.2004

Vadia, S., Tse, J.L., Lucena, R., Yang, Z., Kellogg, D.R., Wang, J.D. et al. (2017) Fatty acid availability sets cell envelope capacity and dictates microbial cell size. *Current Biology*, *27*(12), 1757–67.e5. https://doi.org/10.1016/j.cub.2017.05.076

van den Ent, F., Amos, L.A. & Lowe, J. (2001) Prokaryotic origin of the actin cytoskeleton. *Nature*, *413*(6851), 39–44.

van der Ploeg, R., Verheul, J., Vischer, N.O.E., Alexeeva, S., Hoogendoorn, E., Postma, M. et al. (2013) Colocalization and Interaction Between Elongasome and Divisome During a Preparative Cell Division Phase in *Escherichia coli*. *Molecular Microbiology*, *87*(5), 1074–1087. https://doi.org/10.1111/mmi.12150

Waygood, E.B. & Steeves, T. (1980) Enzyme I of the phosphoenolpyruvate:sugar phosphotransferase system of *Escherichia coli*. purification to homogeneity and some properties. *Canadian Journal of Biochemistry*, *58*(1), 40–48. https://doi.org/10.1139/o80-006

Weart, R.B., Lee, A.H., Chien, A.C., Haeusser, D.P., Hill, N.S. & Levin, P.A. (2007) A metabolic sensor governing cell size in bacteria. *Cell*, *130*(2), 335–347. https://doi.org/10.1016/j.cell.2007.05.043

Weatherspoon-Griffin, N., Zhao, G., Kong, W., Kong, Y., Morigen, Andrews-Polymenis, H. et al. (2011) The CpxR/CpxA two-component system up-regulates two tat-dependent peptidoglycan amidases to confer bacterial resistance to antimicrobial peptide. *The Journal of Biological Chemistry*, *286*(7), 5529–5539. https://doi.org/10.1074/jbc.M110.200352

Westfall, C.S. & Levin, P.A. (2018) Comprehensive analysis of central carbon metabolism illuminates connections between nutrient availability, growth rate, and cell morphology in *Escherichia coli*. *PLoS Genetics*, *14*(2), e1007205. https://doi.org/10.1371/journal.pgen.1007205

Yakhnina, A.A. & Gitai, Z. (2012) The small protein MbiA interacts with MreB and modulates cell shape in *Caulobacter crescentus*. *Molecular Microbiology*, *85*(6), 1090–1104. https://doi.org/10.1111/j.1365-2958.2012.08159.x

Yakhnina, A.A., McManus, H.R. & Bernhardt, T.G. (2015) The cell wall amidase amib is essential for *Pseudomonas aeruginosa* cell division, drug resistance and viability. *Molecular Microbiology*, *97*(5), 957–973. https://doi.org/10.1111/mmi.13077

Yang, D.C., Peters, N.T., Parzych, K.R., Uehara, T., Markovski, M. & Bernhardt, T.G. (2011) An ATP-binding cassette transporter-like complex governs cell-wall hydrolysis at the bacterial cytokinetic ring. *Proceedings of the National Academy of Sciences of the United States of America*, *108*(45), E1052–E1060. https://doi.org/10.1073/pnas.1107780108

Yoshii, Y., Niki, H. & Shiomi, D. (2019) Division-site localization of RodZ is required for efficient Z ring formation in *Escherichia coli*. *Molecular Microbiology*, *111*(5), 1229–1244. https://doi.org/10.1111/mmi.14217

SUPPORTING INFORMATION

Additional supporting information can be found online in the Supporting Information section at the end of this article.

How to cite this article: Sloan, R., Surber, J., Roy, E. J., Hartig, E. & Morgenstein, R. M. (2022). Enzyme 1 of the phosphoenolpyruvate:sugar phosphotransferase system is involved in resistance to MreB disruption in wild-type and Δ*envC* cells. *Molecular Microbiology*, *118*, 588–600. https://doi.org/10.1111/mmi.14988